Dielectric relaxations of poly(acrylic acid)-graft-poly(ethylene oxide) aqueous solution: Analysis coupled with scaling approach and hydrogen-bonding complex

Jingliang Li, Kongshuang Zhao,[*] and Chunyan Liu

College of Chemistry, Beijing Normal University, Beijing 100875, China

Dielectric properties of poly(acrylic acid)-graft-poly(ethylene oxide) (PAA-*g*-PEO) aqueous solution were measured as a function of concentration and temperature over a frequency range of 40 Hz to 110 MHz. After subtracting the contribution of electrode polarization, three relaxation processes were observed at about 20 kHz, 220 kHz, and 4 MHz, and they are named low-, mid- and high-frequency relaxation, respectively. The relaxation parameters of these three relaxations (dielectric increment $\Delta\varepsilon$ and relaxation time τ) showed scaling relations with the polyelectrolyte concentration. The mechanisms of the three relaxations were concluded in light of the scaling theory: The relaxations of low- and mid frequency were attributed to the fluctuation of condensed counterions, while the high-frequency relaxation was ascribed to the fluctuation of free counterions. Based on the dielectric measurements of varying temperatures, the thermodynamic parameters (enthalpy change ΔH and entropy change ΔS) of the three relaxations were calculated and these relaxation processes were also discussed from the microscopic thermodynamical view. In addition, the impacts of PEO side chains on the conformation of PAA-*g*-PEO chains were discussed. PEO side chains greatly strengthen the hydrogen-bonding interactions between PAA-*g*-PEO chains, resulting in the chains overlapping at a very low concentration and the formation of a hydrogen-bonding complex. Some physicochemical parameters of PAA-*g*-PEO molecules were calculated, including the overlap concentration, the effective charge of the chain, the friction coefficient, and the diffusion coefficient of hydrogen counterions.

　　　　　　　　PACS number(s): 61.25.H−, 82.35.−x

I. INTRODUCTION

Poly(acrylic acid)-graft-poly(ethylene oxide) (PAA-*g*-PEO) is a water-soluble, double-hydrophilic grafted copolymer. The nontoxic, hydrophilic PEO side chains change the hydrophilicity of the PAA main chain in water, which increases the mucoadhesive properties of PAA and broadens its application in biomedical fields [1]. Moreover, PAA-*g*-PEO is a typical polyelectrolyte that can interact with metal ions and biological macromolecules through electrostatic force [2]. Because of these facts, PAA-*g*-PEO molecules have drawn much attention in the areas of stabilization of inorganic particles and drug carriers [3–5].

In recent years, extensive attention has been paid to the self-association behaviors of double-hydrophilic copolymers, due to their potential in the field of thickening and pharmaceutical applications [5–8]. Particularly, stimuli-responsive double-hydrophilic copolymers have received ever-increasing interest [9–11], which indicates that such copolymer can be used to prepare novel nanoparticles. As to PAA-*g*-PEO, it has been proved in the works of Han [11] and Tenhu [12] that this copolymer will form hydrogen-bonding complexes in water, owing to the widely existing hydrogen-bonding interactions among carboxyl, amino, and ether-oxygen groups in PAA-*g*-PEO molecules, as shown in Fig. 1. Through controlling the content of PEO side chains [11] and regulating the temperature or *p*H [9,13] of the solution, PAA-*g*-PEO molecules may employ variable conformations, imparting the stimuli-sensitive properties of this copolymer. For PAA-*g*-

PEO, a weak polyelectrolyte, in order to promote its application and provide an understanding of the aggregation behavior and conformation of PAA-*g*-PEO molecules in solution, its physicochemical parameters, electrical properties, and even dielectric properties become important issues worthy of further investigation.

In the last ten years, the scaling concept was widely used to describe the conformation of single polyelectrolyte chain based on the model of electrostatic blobs [14]. It is also important to note that the scaling relations for the chain dimensions of polyelectrolyte complexes as a function of chain length and chain linear charge density were predicted from recent results of molecular dynamics simulations [15–17]; this finding probably reveals the universality of scaling relations in polyelectrolyte systems. On the other hand, many simulation studies about the effect of multivalent counterions on the chain conformation showed that multivalent counterions preferentially condense onto the chain, compared with monovalent counterions [18,19]. The condensed counterions will form dipoles with the monomer and the resulting attractive dipole-dipole interactions usually induce the collapse of charged polyelectrolyte chains [20,21]. These findings show that counterions play an important role in determining the chain conformation. Relatively, experimental research of the conformation of polyelectrolyte chain and the distribution of counterions are somewhat backward. Very recently, Duhamel and co-workers [22] reported a surprising finding by fluorescence quenching experiments that metal cations bind to a polyelectrolyte by distributing themselves randomly into an array of self-defined subdomains of dimension equal to the Debye length. This result should prove valuable to scientists interested in characterizing the complex behavior of polyelectrolytes. Therefore, it is meaningful to experimentally explore the effect

————————
[*]Corresponding author: College of Chemistry, Beijing Normal University, Beijing, China; zhaoks@bnu.edu.cn
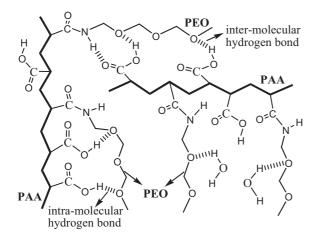
FIG. 1. Structure of PAA-*g*-PEO molecule. PEO side chains are grafted to PAA main chain by amide bond; inter- and intrahydrogen bonds (dashed lines) widely exist in PAA-*g*-PEO solution.

of various interactions, such as electrostatic and hydrophilic interactions, on the conformation of polyelectrolyte chain.

In this work, we employed the method of dielectric relaxation spectroscopy (DRS), which represents a powerful tool that provides information not only on the static conformation and electric properties of the polyelectrolyte system, but also on the motion of molecules, ion diffusion, and changes of dipole movement [23–26]. For this reason, a number of studies by DRS have been focused on the polyelectrolyte solutions [23–26]. Among these works, the scaling theory of fluctuation of counterions [23,25] and Manning's counterion condensation model [27] were successfully applied to explore structural and dynamical problems of the polyelectrolyte solutions.

As a common feature of most polyelectrolyte solutions, two dielectric relaxations can generally be observed below GHz: One at lower frequencies (around kHz) is thought to be the fluctuation of condensed counterions [23,26], and the other (between 1 and 100 MHz) is still under controversy [23]. In addition, there are a few reports [26,28,29] that three relaxations in polyelectrolyte solutions are observed within the radiofrequency range, which may be due to the difficulty to analysis the dielectric spectra, at least in part because the electrode polarization (EP) effect often obscures the relaxation at low frequency [23], and it is hard to decompose overlapped relaxations and justify their responsible mechanisms. Therefore, to identify the mechanisms of the two relaxations reported and to confirm whether the PEO side chains will cause new relaxation processes, and also to investigate the problems of counterions distribution and the conformation of PAA-*g*-PEO chains, the dielectric measurement of PAA-*g*-PEO solutions is meaningful.

More recently, we have investigated the dynamic behaviors of aqueous PAA-*g*-PEO-7% (the weight percent of PEO) solutions with different counterions (Na$^+$, K$^+$, and NH$_4{}^+$) by DRS [29]. It was also observed that the scaling behaviors between the dielectric parameters and the concentration vary with the counterions, indicating the counterions affect the conformation of polyelectrolyte chain. Compared with PAA-*g*-PEO-7%, the copolymer in this work contains almost double-PEO side chains (up to 13%) and is named

PAA-*g*-PEO-13%. In PAA-*g*-PEO-13% solutions, the stronger hydrogen-bonding interactions will lead to the formation of more and larger complexes [11]. In addition, the interactions in PAA-*g*-PEO-13% solutions are relatively simple as no extra counterions were introduced, because added ions strongly screen the Coulomb repulsion between charged monomers and influence the chain conformation [30,31]. In this work, we focused on the effects of PEO side chains and hydrogen-bonding interactions on the conformation of PAA-*g*-PEO chains and their dielectric behaviors.

To this end, dielectric properties of PAA-*g*-PEO solution were measured as a function of concentration and temperature from 40 Hz to 110 MHz. Mechanisms of the relaxations were analyzed via the scaling theory of the fluctuation of counterions. In addition, the activation enthalpies and entropy changes of each relaxation process were calculated from the temperature-dependent spectra, and the relaxations were discussed from the microscopic thermodynamical view.

II. EXPERIMENTAL DETAILS

A. Materials and preparation of PAA-*g*-PEO-13% solutions

Materials. Poly(acrylic acid) (PAA) aqueous solution (weight fraction 35%, Mw 2.5×10^5 g/mol) from Sigma-Aldrich was used without further purification. Ethylene oxide (EO) from Beijing Chemical Reagents Co., Ltd., was purified by distillation with CaH$_2$ and KOH, and was stored in an atmosphere of Ar at $-18\,^\circ$C. PEO [Mw 2.0×10^3 g/mol, determined by ^{1}H nuclear magnetic resonance (NMR) and gel permeation chromatography (GPC) measurements] with a primary amine group was prepared using potassium bis(trimethylsilyl)amide ([(CH$_3$)$_3$Si]$_2$NK) as the initiator. PAA-*g*-PEO-13% was prepared according to the classical reaction of amino with carboxylic groups in the presence of *N*-(3-(dimethylamino)propyl)-*N*-ethylcarbo-diimide hydrochloride and 1-hydroxybenzotrizole (from Shanghai Medpep Co., Ltd.); the preparing method has been already reported elsewhere [11]. The crude product of PAA-*g*-PEO-13% was dialyzed against distilled water for 4 days and then lyophilized. The composition and molecular weight of the copolymer were determined by ^{1}H NMR measurements.

PAA-*g*-PEO-13% solutions were prepared by dissolving a known amount of sample in a given volume of doubly distilled water (specific resistance higher than 16 MΩ/cm). Diluted by double-distilled water directly, solutions of different concentration from 8.0 to 0.01 mg/ml were obtained.

B. Dielectric measurements

Dielectric measurements of PAA-*g*-PEO-13% solutions were carried out on a 4294A Precision Impedance Analyzer (Agilent Technologies) that allows a continuous frequency measurement from 40 Hz to 110 MHz, controlled by a personal computer. The applied alternating field was 500 mV and the temperature (from 6.9 °C to 86.4 °C) of the samples was controlled by a circulating thermostated water jacket. A dielectric measuring cell with concentrically cylindrical platinum electrodes was employed to load the samples; the effective area of the electrodes was 78.5 mm^2 and the electrode distance was 8 mm. All the experimental data

were corrected for errors arising from stray capacitance (C_r) and the cell constant (C_l), they are 0.434 and 0.663 pF, respectively, determined with pure water, ethanol, and air. The residual inductance (L_r) arising from the connecting leads was determined by using KCl solution with different concentrations through the relation $C_x = L_r G_x^2$, where C_x and G_x denote the measured capacitance and conductance, respectively. The raw data measured were corrected according to Schwan's method [32,33], based on the following equations:

$$C_s = \frac{C_x(1 + \omega^2 L_r C_x) + L_r G_x^2}{(1 + \omega^2 L_r C_x)^2 + (\omega L_r G_x)^2} - C_r, \qquad (1)$$

$$G_s = \frac{G_x}{(1 + \omega^2 L_r C_x)^2 + (\omega L_r G_x)^2}, \qquad (2)$$

where C_s and G_s denote the modified capacitance and conductance, respectively. $\omega (= 2\pi f; f$ is the measurement frequency) is the angular frequency. The values of permittivity $\varepsilon' = C_s/C_l$ and conductivity $\kappa = G_s \varepsilon_0/C_l$ were obtained from the corrected capacitance and conductance, where ε_0 is the permittivity of vacuum.

C. Dielectric analysis

In an applied electric field of frequency f, the dielectric property of an aqueous polyelectrolyte solution is generally characterized in terms of the complex permittivity ε^* defined as

$$\varepsilon^* = \varepsilon' - \frac{j\kappa}{\omega\varepsilon_0} = \varepsilon' - j\left(\varepsilon'' + \frac{\kappa_l}{\omega\varepsilon_0}\right), \qquad (3)$$

where ε' and κ are the permittivity and the conductivity of the system, κ_l is the low-frequency limit of conductivity, and $j = (-1)^{1/2}$. The dielectric loss ε'' was calculated from the conductivity spectra through the equation $\varepsilon'' = (\kappa - \kappa_l)/\omega\varepsilon_0$, where κ_l was read out from the conductivity spectra at low frequency.

The whole dielectric spectrum was analyzed using an empirical equation including the Cole-Cole function and the EP term [33]:

$$\varepsilon^* = \varepsilon_h + \sum_i \frac{\Delta\varepsilon_i}{1 + (j\omega\tau_i)^{\alpha_i}} + A\omega^{-m} + jB\omega^{-n}, \qquad (4)$$

where i is the number of relaxations, ε_h denotes the high-frequency limits of permittivity, $\Delta\varepsilon(=\varepsilon_l - \varepsilon_h)$ the dielectric increment, $\tau(=1/2\pi f_0)$ the characteristic relaxation time (f_0 is characteristic relaxation frequency), $\alpha(0 < \alpha < 1)$ the parameters indicating the distribution of relaxation times and the shape of relaxation peaks. The terms $A\omega^{-m}$ and $B\omega^{-n}$ (A, B, m, and n are adjustable parameters) in Eq. (4) take into account the effect of electrode polarization (EP) on the real and imaginary part of the permittivity, respectively, on the basis of the power-law frequency dependence method [33]. This is because in our study, the high conductivity of PAA-g-PEO solutions causes a giant EP which may mask the relaxation behavior at low-frequency range.

By fitting the expression Eq. (4), including both the electrode polarization and the effective dielectric relaxation, to the raw experimental data over the whole frequency range, the EP term ($A\omega^{-m}$ and $B\omega^{-n}$) and the dielectric parameters of each relaxation process can be determined [32].

III. MODEL AND THEORY

A. Model for the conformation of polyelectrolyte

A scaling model for the conformation of polyelectrolyte proposed by de Gennes *et al.* [34] has been successfully applied to study the dynamics of polyelectrolyte solution [14,23,30]. In most solutions, polyelectrolyte chains are locally collapsed inside the electrostatic blobs, shielding as many monomers as possible from the unfavorable interaction with solvent. Inside electrostatic blobs, electrostatic repulsion competes with thermodynamic interaction between polymer and solvent to determine the chain configuration. The physics image about the conformation of polyelectrolyte chain can be understood by the following schematic representation given in Fig. 2.

In this model, each electrostatic blob is of size ξe and contains ge monomers. In dilute solution, the polyelectrolyte chain adopted an extended rodlike configuration of electrostatic blobs with length L [see Fig. 2(a)]. The chain contour length L is smaller than the distance between the chains R_{cm} and is determined by the electrostatic repulsion between the N/ge electrostatic blobs:

$$L \approx \frac{N}{ge}\xi e \text{ dilute solution}, \qquad (5)$$

where N is the polymerization degree of polyelectrolyte chain. R_{cm} has a power-law relationship with concentration c (the number density of monomers):

$$R_{cm} \approx \left(\frac{N}{c}\right)^{1/3} \text{ dilute solution}. \qquad (6)$$

As the concentration of polyelectrolyte increases to the overlap concentration c^*, the chains touch one another and the distance R_{cm} between the chains become equal to their extended size L. The overlap concentration c^* is given by

$$c^* \approx \frac{(ge/\xi e)^3}{N^2}. \qquad (7)$$

In semidilute solutions (concentration $c > c^*$), the major feature is the existence of the correlation length ξ [see Fig. 2(b)] and electrostatic interactions are screened on length
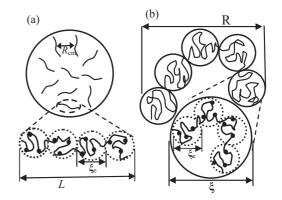

FIG. 2. Structures of polyelectrolyte chains in (a) dilute solution; R_{cm} denotes the distance between chains, L the length of electrostatic blobs, and ξe the diameter of electrostatic blob; (b) semidilute solution; R and ξ denote the end-to-end distance and the correlation length of polyelectrolyte chains, respectively.

scales larger than ξ. The correlation length ξ shows a power-law relationship with concentration c:

$$\xi \approx \left(\frac{ge}{c\xi e}\right)^{1/2} \quad \text{semidilute,} \quad (8)$$

and the chain is a random walk of blobs with end-to-end distance R, which is represented as

$$R \approx \left(\frac{\xi e}{cge}\right)^{1/4} N^{1/2} \quad \text{semidilute.} \quad (9)$$

B. Counterion polarization theory: Ito model

As is well known, polyelectrolytes are macromolecules with many ionizable groups; part of these groups dissociate in aqueous solutions, leaving fixed charges on the polyelectrolyte chain and counterions in the bulk solution. According to Manning's condensation theory [27], some counterions in polyelectrolyte solution will condense near the fixed charges to partially neutralize the excess charges when $l_B/b > 1$; here b is the average spacing between charged groups on the polyelectrolyte chain, l_B is the Bjerrum length ($l_B = e^2/4\pi\varepsilon_m k_B T$, ε_m is the permittivity of solvent, e the elemental charge, k_B the Boltzmann constant, and T the Kelvin temperature). Therefore, there are two kinds of bound counterions: One is tightly bound in the vicinity of the fixed charge on the chain and is called the "condensed counterion"; the other is loosely bound within a wide range between the chains and here is called the "free counterion". The number of the condensed counterions can be expressed by $1 - f = 1 - b/l_B$, where f is the fraction of free counterions in all the counterions. The distribution of free and condensed counterions is schematically shown in Fig. 3. The condensed counterions are trapped by a periodically electrostatic potential along the chain, where the period corresponds to the average distance between two adjacent charges on the chain. The free counterions are trapped by screened Coulombic force ψ owing to the shielding effect of the condensed counterions [24–26].
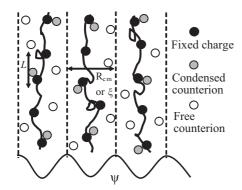

FIG. 3. The distribution of free counterions (open circle) and condensed counterions (gray filled circle) in polyelectrolyte solution; the black filled circle represents the fixed charge. The free counterions are trapped by the screened electrostatic potential ψ that comes to a minimum at the fixed charge. The condensed counterions fluctuate along the chain within the distance equal to the chain contour length, L; the free counterions fluctuate perpendicular to the polyelectrolyte chain, within the distance between two dashed lines that equals R_{cm} in dilute solutions or ξ in semidilute solutions (see in Fig. 2).

On one hand, according to Ito's counterion polarization model [23,25,26], the condensed counterions fluctuate along the polyelectrolyte chain as indicated by the arrow of Fig. 3, causing polarization over a length scale comparable to the end-to-end distance of the chain [corresponding to L in Fig. 2(a) for dilute solutions and R in Fig. 2(b) for semidilute solutions]. The dielectric increment $\Delta\varepsilon_{\text{cond}}$ (subscript *cond* represents condensed counterions), produced by the polarization of condensed counterions, can be approximated as the product of the induced dipole moment of a single chain (μ_{cond}) and the number density of chains (c/N):

$$\Delta\varepsilon_{\text{cond}} \approx \frac{c}{N}\mu_{\text{cond}} \approx \frac{c}{N}\frac{(1-f)Ne^2}{k_B T}L^2 \quad \text{dilute,} \quad (10a)$$

$$\Delta\varepsilon_{\text{cond}} \approx \frac{c}{N}\frac{(1-f)Ne^2}{k_B T}R^2 \quad \text{semidilute.} \quad (10b)$$

Substituting Eq. (5) into Eq. (10a) [or Eq. (9) into Eq. (10b)] and combining with Eq. (7), the following equation that shows scaling relations between $\Delta\varepsilon_{\text{cond}}$ and concentration c can be obtained:

$$\Delta\varepsilon_{\text{cond}} \approx \frac{(1-f)e^2}{k_B T}\frac{ge}{\xi e}\frac{c}{c^*} \quad \text{dilute,} \quad (11a)$$

$$\Delta\varepsilon_{\text{cond}} \approx \frac{(1-f)e^2}{k_B T}\frac{ge}{\xi e}\left(\frac{c}{c^*}\right)^{1/2} \quad \text{semidilute.} \quad (11b)$$

The relaxation time τ_{cond} of condensed counterions is insensitive to the concentration of polyelectrolyte [23], and is determined by the chain contour length L and the friction coefficient ζ for condensed counterions moving along the polyelectrolyte chain:

$$\tau_{\text{cond}} = \frac{\zeta L^2}{6k_B T} = \frac{\zeta}{6k_B T}\left(\frac{N\xi e}{ge}\right)^2 \quad \text{dilute and semidilute.}$$

$$(12)$$

Combining Eq. (11a) with Eq. (12), ζ can be obtained from the following formula:

$$\zeta = 6(1-f)ce^2\frac{\tau_{\text{cond}}}{\Delta\varepsilon_{\text{cond}}}. \quad (13)$$

On the other hand, the free counterions fluctuate in the directions perpendicular to the chain backbone, within the distance R_{cm} in dilute solutions and ξ in semidilute solutions (see Fig. 3) [24–26]. The dielectric increment $\Delta\varepsilon_{\text{free}}$ (subscript *free* represents free counterions) caused by this polarization can be represented by the product of the number density of free counterions fc and their polarizability μ_{free}. Substituting Eq. (6) or Eq. (8) into $\Delta\varepsilon_{\text{free}} \approx fc\mu_{\text{free}}$, the relations between $\Delta\varepsilon_{\text{free}}$ and concentration c can be obtained as

$$\Delta\varepsilon_{\text{free}} \approx fc\frac{e^2 R_{cm}^2}{k_B T} \approx \frac{fe^2 N^{2/3}}{k_B T}c^{1/3} \quad \text{dilute,} \quad (14a)$$

$$\Delta\varepsilon_{\text{free}} \approx fc\frac{e^2\xi^2}{k_B T} \approx \frac{fe^2 ge}{k_B T\xi e} \quad \text{semidilute.} \quad (14b)$$

The relaxation time τ_{free} of free counterions is related to the diffusion coefficient of counterions D and the fluctuation distance [corresponding to R_{cm} in Eq. (6) and ξ in Eq. (8)].

The expressions of τ_{free} for the dilute solution and semidilute solution are given by

$$\tau_{\text{free}} \approx \frac{R_{cm}^2}{6D} \approx \frac{N^{2/3}}{6Dc^{2/3}} \quad \text{dilute}, \tag{15a}$$

$$\tau_{\text{free}} \approx \frac{\xi^2}{6D} \approx \frac{ge}{6D\xi ec} \quad \text{semidilute}. \tag{15b}$$

As to the relaxations caused by free counterions, the following relation can be deduced by combining Eq. (14) with Eq. (15) for both dilute and semidilute solutions:

$$\ln \Delta \varepsilon_{\text{free}}/\tau_{\text{free}} \approx \ln c + \ln \frac{6Dfe^2}{k_B T}. \tag{16}$$

It is obvious that $\Delta \varepsilon_{\text{free}}/\tau_{\text{free}}$ varies linearly with c in a slope close to unity. In addition, another expression for D was also derived from Eqs. (14) and (15):

$$D \approx \frac{k_B T}{6fce^2} \frac{\Delta \varepsilon_{\text{free}}}{\tau_{\text{free}}} = \frac{1}{6fl_B \varepsilon_m c} \frac{\Delta \varepsilon_{\text{free}}}{\tau_{\text{free}}}. \tag{17}$$

Each polyelectrolyte bears an effective charge Q_P,

$$Q_P = z_P e N f, \tag{18}$$

where z_P is the valence of the fixed charged group on a polyelectrolyte chain.

IV. RESULTS AND DISCUSSION

A. Concentration dependence of dielectric spectra of PAA-*g*-PEO solutions

Figure 4 shows the dielectric spectra of PAA-*g*-PEO aqueous solutions of different concentrations at 20.9 °C. From Fig. 4, a widely distributed relaxation can be observed in the frequency range from 100 kHz to 100MHz, and the frequency of this relaxation increases with concentration as shown by the arrow. Moreover, it should be noted that the steep rise in permittivity at low frequency is attributed to the effect of electrode polarization (EP), which should be removed from the spectra before dielectric analysis because the EP often obscures the relaxations in the low-frequency range [23,32].

FIG. 4. Three-dimensional plots of dielectric permittivity as functions of frequency and concentration of PAA-*g*-PEO solution at 20.9 °C.

1. Determination of dielectric parameters

In order to remove the effect of EP and confirm the mechanisms of relaxations that were included in the widely distributed relaxation spectra, Eq. (4)—including three Cole-Cole relaxation terms and the electrode polarization terms $A\omega^{-m}$ and $B\omega^{-n}$ which take into account the effect of EP on the real and imaginary part of the permittivity—was used to fit the dielectric spectra of PAA-*g*-PEO solutions. To ensure the reliability of the fitting results, a multistep fitting procedure was employed. Figure 5 shows a representative fitting result of concentration 0.6 mg/ml in this way. Firstly, we fit the raw ε' curve and the ε'' curve free of the contribution of dc conductivity, so that the EP term ($A\omega^{-m}$ and $B\omega^{-n}$) and the rough dielectric parameter ($\Delta \varepsilon$ and τ, etc.) were determined. Then, new ε' and ε'' curves free of the EP effect were derived by mathematically subtracting $A\omega^{-m}$ from the permittivity and the $B\omega^{-n}$ from the dielectric loss, respectively. Finally, fitting simultaneously the new ε' and ε'' curves, the effective dielectric parameters of the relaxations were determined [32]. The optimized fitting curve was guaranteed by the nonlinear least-squares method.

It can be clearly seen from Fig. 5 that the solid lines well describe the corrected values of the permittivity and the dielectric loss according to Eq. (4), and the EP effect (circled by a dashed ring) was well eliminated. Similar results were also found for other PAA-*g*-PEO solutions and the obtained dielectric parameters are listed in Table I. Theses results show that the dielectric spectra with a broad distribution include three relaxation processes in the studied frequency range. For simplicity, we call these three relaxations subrelaxation 1, subrelaxation 2, and subrelaxation 3 from low to high frequency, respectively, whose dielectric increments and characteristic times are defined as $\Delta \varepsilon_1$, $\Delta \varepsilon_2$, $\Delta \varepsilon_3$, and τ_1, τ_2, τ_3, respectively.

2. Mechanism of dielectric relaxation

As described in the Introduction, within the frequency range in our study (40 Hz to 110 MHz), two dielectric relaxations can

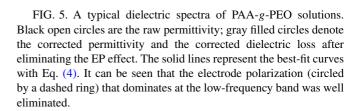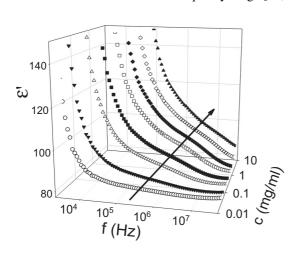FIG. 5. A typical dielectric spectra of PAA-*g*-PEO solutions. Black open circles are the raw permittivity; gray filled circles denote the corrected permittivity and the corrected dielectric loss after eliminating the EP effect. The solid lines represent the best-fit curves with Eq. (4). It can be seen that the electrode polarization (circled by a dashed ring) that dominates at the low-frequency band was well eliminated.

TABLE I. Dielectric parameters of the relaxations in PAA-*g*-PEO solutions of different concentrations, obtained by fitting Eq. (4) to the experimental data.

c (mg/ml)	$\Delta\varepsilon_1$	$\Delta\varepsilon_2$	$\Delta\varepsilon_3$	τ_1 (μs)	τ_2 (μs)	τ_3 (ns)	α_1	α_2	α_3
0.01	1.15	0.292	0.174	7.21	0.766	104	0.92	0.99	0.99
0.03	2.70	1. 80	0.965	7.25	0.757	122	0.94	0.93	0.98
0.06	7.46	2.70	3.46	7.24	0.758	96.6	0.94	0.96	0.92
0.15	16.5	5.10	8.41	7.20	0.822	74.4	0.92	0.90	0.82
0.3	25.3	10.0	10.0	7.57	0.800	48.0	0.88	0.74	0.81
0.6	34.4	14.0	14.0	7.20	0.691	31.9	0.91	0.83	0.85
1.0	44.6	18.0	17.1	7.26	0.569	21.0	0.91	0.84	0.82
2.0	20.6	11.3	14.5	0.971	0.138	11.1	0.99	0.95	0.93
4.0	22.3	14.6	9.89	0.561	0.0684	6.90	0.87	0.84	0.99
8.0	20.5	21.1	8.94	0.339	0.0502	3.65	0.98	0.88	0.94

generally be observed in polyelectrolyte solutions. It is worthy to note that three relaxations were confirmed in this work, which is not an easily found phenomenon. The additional relaxation in PAA-*g*-PEO solutions is related to the existence of hydrogen-bonding complexes, which will be discussed later.

As to the relaxations due to the polarization of condensed counterions, the scaling behaviors of the dielectric parameters, such as the dielectric increment $\Delta\varepsilon_{cond}$ and the relaxation time τ_{cond}, can be described by Eqs. (11) and (12). To identify the mechanism of the relaxations, $\Delta\varepsilon_i$ and τ_i were plotted as a function of the concentration c in Fig. 6. From Fig. 6, two breaks in $\Delta\varepsilon_i$ and τ_i can be observed at $c \approx 0.2$ mg/ml and $c \approx 1.2$ mg/ml, which divide the concentration range into three regions marked as regions I, II, and III, respectively. The overlap concentration c^* between regions I and II can be clearly recognizable in Fig. 6. The scaling exponents in these three regions display different values marked with numbers, and the values are listed in Table II, together with those predicted from the scaling theory.

a. Low-frequency subrelaxation 1. From Table II, it is clear that for subrelaxation 1 the scaling exponents obtained experimentally are in good agreement with those predicted from the scaling theory of condensed counterions, whether in dilute solution or in semidilute solution; namely, the value of dielectric increment, 1.010 (experimental), is approximately equal to 1 (theoretical) for dilute solution, and 0.469–0.5 for
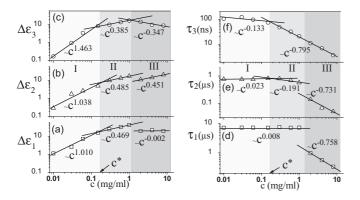
semidilute solution. The value of relaxation time, 0.008, is near 0 for both dilute and semidilute solution. Therefore, it can be concluded that subrelaxation 1 is caused by the fluctuation of condensed counterions along the PAA-*g*-PEO chain (see Fig. 3), which is in agreement with the literature [23,25,26].

Obviously, regions I and II in Fig. 6 belong to dilute and semidilute solution according to Eqs. (12a) and (12b), while region III is yet to be defined. It should be noted that the scaling behaviors in region III differentiate largely from those in regions I and II; this is likely to indicate that the chain conformation changed significantly in region III. According to Rubinstein *et al.* [30], the semidilute solution was divided into unentangled and entangled semidilute regimes, and the entanglement criterion is that significant overlap of the chains is required for them to begin topologically constraining each other's motion. From the results of dynamic light scattering in Han's work [11], which showed there are a large number of intermolecular hydrogen-bonding complexes in PAA-*g*-PEO solutions of concentration 1 mg/ml, we can conclude that PAA-*g*-PEO chains in region III significantly entangle with each other. Hence, it may be deduced that the region II in this work should be called unentangled semidilute solution, and the region III called entangled semidilute solution, respectively. The conformation of PAA-*g*-PEO chains with increasing concentration was schematically shown in Fig. 7. Additionally, it is interesting to note that for PAA-*g*-PEO, the ratio of entanglement concentration and overlap concentration c_e/c^*, which is approximately equal to 6 ($\approx 1.2/0.2$), greatly deviated from the predicted value for polyelectrolyte (10^3–10^4) [30], while it is in good agreement with the predicted value for neutral polymers (5–10). This finding suggests that the PAA-*g*-PEO chains behave like neutral polymers; namely, the unentangled semidilute regime covers a narrow range of concentration. This result can be interpreted by the following facts: In semidilute solutions, many carboxyl groups on the PAA main chain participated to form hydrogen bonds with PEO side chains, and meanwhile only a small amount of carboxyl groups ionized because PAA-*g*-PEO is a weak polyelectrolyte. As a result, the charge density of the PAA-*g*-PEO chain is very low.

b. Middle-frequency subrelaxation 2. In Table II, it can also be seen that in the concentration range from 0.01 to 1.0 mg/ml, the scaling exponents of the subrelaxation 2 are reasonably in agreement with those values predicted from the scaling theory of condensed counterions: the dielectric increment, 1.038

FIG. 6. The scaling behaviors of dielectric increment (a)–(c) and relaxation time (d)–(f) of three subrelaxations as a function of concentration c. The concentration range is divided into three regions: regions I, II, and III according to different scaling behaviors.

TABLE II. Values of scaling exponents determined by this work (see in Fig. 6) and those theoretical values predicted from Eqs. (11), (12), (14), and (15), respectively.

		Condensed counterions		Free counterions	
		$\Delta\varepsilon_{\text{cond}}$	τ_{cond}	$\Delta\varepsilon_{\text{free}}$	τ_{free}
Theoretical values	Dilute	1	0	1/3	$-2/3$
	Semidilute	0.5	0	0	-1
		Subrelaxation 1		Subrelaxation 2		Subrelaxation 3	
		$\Delta\varepsilon_1$	τ_1	$\Delta\varepsilon_2$	τ_2	$\Delta\varepsilon_3$	τ_3
Experimental values	Dilute	1.010	0.008	1.038	0.023	1.463	-0.133
	Semidilute	0.469	0.008	0.485	-0.191	0.385	-0.795

(experimental), is near to 1 (theoretical) for dilute solution, and 0.485–0.5 for semidilute solution; the relaxation time, 0.023, is near 0 for dilute solution, and -0.191 deviates a little from 0 for semidilute solution. Therefore, an analogous conclusion, that subrelaxation 2 also originates from the fluctuation of condensed counterions, can be drawn.
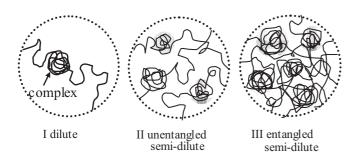
According to Eq. (12) of Ito's theory [25,26], the relaxation time of condensed counterions is determined by their fluctuation distance that equals the contour length of the chain. The above conclusions about the mechanisms of the subrelaxation 1 and subrelaxation 2 suggest there are two kinds of fluctuation distance for the movement of condensed counterions. The subrelaxation 2 occurs at higher frequency (at about 220 kHz) compared with the subrelaxation 1, and this relaxation frequency is also higher than that of condensed counterions reported in the literature [23,25,26]. Therefore, it can be concluded that subrelaxation 2 fluctuates with a shorter distance than subrelaxation 1. Considering the existence of hydrogen-bonding complexes (see Fig. 7) within which the charge density of counterions is large, it can be predicted that when the condensed counterions move along the chain, the strong electrostatic repulsion in the complex will prevent the counterions from crossing through. Therefore, a part of the condensed counterions fluctuating along PAA-*g*-PEO chains are blocked by the complexes and restricted within a shorter distance, which results in the occurrence of subrelaxation 2.
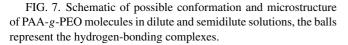
c. High-frequency subrelaxation 3. As to the controversial relaxation around MHz, the scaling law proposed by Ito *et al.* [23,25] point out that the fluctuation of free counterions caused this relaxation, which was well proved by recent works [24,29,32]. Therefore, we speculate the subrelaxation 3 in this work (from 1.2 to 43.6 MHz, obtained from Table I) probably originates from H^+ free counterions. With regard to the relaxations caused by the fluctuation of free counterions, the scaling relationship $\Delta\varepsilon_{\text{free}}/\tau_{\text{free}} \propto c^1$ is expected by Eq. (16). From Fig. 8, the double-logarithmic plot of $\Delta\varepsilon_3/\tau_{03}$ against c, it can be seen that the scaling exponent 1.031 (experimental) approximately equals 1 (theoretical). The above results give support to the hypothesis that the subrelaxation 3 is due to the fluctuation of free counterions.

Additionally, the subrelaxation 3 should also be connected to PEO side chains and the hydrogen-bonding complexes in solution, because there are some discrepancies between the scaling exponents from our experiments and the values from the scaling theory of free counterions (seen in Table II). These discrepancies may be due to the large number of hydrogen bonds among PAA-*g*-PEO chains, which probably bring deviation to the scaling behaviors between the distance between chains (or the correlation length) and the concentration, referring to Eqs. (6) and (8). Consequently, the scaling behaviors for both the dielectric increment and the relaxation time of subrelaxation 3 deviate partly from the theoretical descriptions in Eqs. (14) and (15).

In conclusion, mechanisms of the three subrelaxations have been proved by means of the scaling theory; both subrelaxation 1 (around 20 kHz) and subrelaxation 2 (around 220 kHz) were caused by the fluctuation of condensed counterions, and the subrelaxation 3 (around MHz) was due to the fluctuation of free counterions, respectively. It is in agreement with the conclusion about the mechanism of the relaxations in PAANa
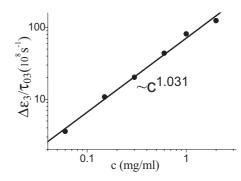

FIG. 7. Schematic of possible conformation and microstructure of PAA-*g*-PEO molecules in dilute and semidilute solutions, the balls represent the hydrogen-bonding complexes.

FIG. 8. Double-logarithmic plot of $\Delta\varepsilon_3/\tau_{03}$ against c, the solid line is the linear fitting result whose slope is also presented.

solution [35,36]. The additional relaxation observed in PAA-*g*-PEO solutions as compared to PAANa solutions is related to the hydrogen-bonding complexes. In addition, it can be seen from Fig. 6 that for each subrelaxation the scaling behaviors in region III are distinguishable from those in regions I and II; this indicates PEO side chains and hydrogen-bonding complexes greatly affect the conformation and the dielectric behaviors of PAA-*g*-PEO molecules at higher concentrations.

3. Physicochemical parameters of PAA-g-PEO molecules in solution

By means of the scaling theory, the information on the relaxation mechanisms in PAA-*g*-PEO solutions was achieved. In addition, some physicochemical parameters characterizing the molecule configuration, intramolecular and intermolecular interactions, and dynamic behavior were also estimated. From the breakpoint between regions I and II in Fig. 6, the overlap concentration c^* was obtained. According to Eqs. (7) and (11), the fraction of free counterions f in both dilute and semidilute solutions was estimated. Then, the friction coefficient $\zeta(H^+)$ of condensed counterions moving along the chain was obtained by substituting $\Delta\varepsilon_1$ and τ_1 (from Table I) into Eq. (13), and the diffusion coefficient of counterions $D(H^+)$ was calculated by substituting $\Delta\varepsilon_3$ and τ_3 into Eq. (17). Also, the electric information of PAA-*g*-PEO chains Q_P in Eq. (18) was acquired. The calculated results of $\zeta(H^+)$, Q_P, and $D(H^+)$ with varying concentration are listed in Table III. noting that in region III these physicochemical parameters cannot be obtained through the scaling theory, because the theory is no longer applicable.

The overlap concentration c^* of PAA-*g*-PEO-13% solution was determined to be 0.187 mg/ml (see Fig. 6); it is one order of magnitude smaller than that of PAA (Mw: 2.5×10^5 g/mol) which is about 9.1–10 mg/ml obtained from the viscosity and dynamic light scattering measurements in Litmanovich's work [37]. This result is quite predictable because PEO side chains greatly strengthen the interactions among PAA-*g*-PEO chains [11,12]; thus PAA-*g*-PEO molecules start to overlap at very low concentrations. The overlap concentration is a fundamental parameter describing the thickening properties of macromolecules; upon the c^* the viscosity of the solution changes dramatically [30,38]. The low c^* of PAA-*g*-PEO solution indicates this copolymer exhibits good thickening abilities owing to PEO side chains.

TABLE III. Some physicochemical parameters of PAA-*g*-PEO molecules.

c (mg/ml)	$\zeta(H^+)$ (10^{-11} kg/s)	Q_P (10^{-16} C)	$D(H^+)$ (10^{-10} m^2/s)
0.01	1.26	5.479	0.680
0.03	1.24	5.498	1.07
0.06	1.24	5.473	2.44
0.15	1.35	5.483	3.07
0.3	1.66	5.486	2.83
0.6	2.03	5.488	2.98
1.0	2.16	5.488	3.32

The friction coefficient $\zeta(H^+)$ was calculated from Eq. (13) and its mean value equals 1.56×10^{-11} kg/s. This value is larger than the friction coefficient of other monovalent ions (Li$^+$, Na$^+$, and I$^+$) that is about 5.0×10^{-12} kg/s in Koneshan's work [39] from computer simulation. It suggests the movement of hydrogen ions suffers greater resistance, because hydrogen ions are in the hydrated form in solution. It should be noted in Table III that in dilute solutions (0.01–0.15 mg/ml), the value of $\zeta(H^+)$ changes little with concentration, indicating the movement of hydrogen ions was free from the electrostatic forces of fixed charges on other polyelectrolyte chains, because the chains in dilute solutions are far from each other. In semidilute solutions (0.3–1.0 mg/ml), however, the $\zeta(H^+)$ increases with concentration, because hydrogen ions suffer from the electrostatic forces from other chains. Moreover, the diffusion coefficient of hydrogen counterions $D(H^+)$ was estimated from Eq. (17) to be about 2.32×10^{-10} m^2/s (from Table III). However, it is too small compared with that in water 9.311×10^{-9} m^2/s [40]. This large discrepancy may result from the deviation of the scaling behaviors of subrelaxation 3 and the scaling theory of free counterions, namely Eqs. (14) and (15).

Additionally, the effective charge Q_P on each polyelectrolyte chain was obtained (see Table III). The Q_P is in correlation to the information of effective charge density, the distribution of counterions, and also the flexibility of the chain [15].

B. Temperature dependence of dielectric spectra of PAA-g-PEO solutions

In the above sections, the dielectric analyses for the PAA-*g*-PEO solutions with varying concentrations have been carried out at a constant temperature of 20.9 °C, and mechanisms of the observed three relaxation processes were also identified. As is well known, temperature regulates the hydrophilicity of macromolecular chain, changes the viscosity and permittivity of solvent medium, and affects the distribution of counterions. Moreover, temperature can accelerate thermal motion of molecules and ions, and especially can break hydrogen bonds. Therefore, studying the dielectric behaviors of PAA-*g*-PEO solutions under varying temperatures is significant to detect the conformational changes and the dynamics in polyelectrolyte solutions. Based on these understandings, the dielectric measurements at different temperatures were carried out on some selected solutions, namely, 0.01, 0.3, 0.6, and 2.0 mg/ml.

1. Analysis of the dielectric spectra

A widely distributed relaxation similar to that in Fig. 4 was observed in the dielectric spectra of PAA-*g*-PEO solutions at different temperatures. Analogously, the dielectric data were fitted by using Eq. (4). For the dielectric data of temperature range 6.9 °C–49.3 °C, the Cole-Cole equation with three relaxation terms was used, while for the data of 62.2 °C–86.4 °C, the equation with two relaxation terms was used. The fitting results are listed in Table IV, and for all solutions the number of relaxations showed the same changing trend with temperature: At lower temperature range, three subrelaxations exist, called subrelaxation 1, subrelaxation 2, and subrelaxation 3 as previously described; but at higher

TABLE IV. The dielectric parameters obtained by fitting Eq. (4) to experimental data of PAA-g-PEO solution of concentration 0.6 mg/ml at different temperatures.

t (°C)	$\Delta\varepsilon_1$	$\Delta\varepsilon_2$	$\Delta\varepsilon_3$	τ_1 (μs)	τ_2 (μs)	τ_3 (ns)
6.9	27.9	18.9	10.0	7.59	0.810	42.7
20.9	31.2	14.1	14.3	7.26	0.804	30.7
34.0	18.9	18.4	9.33	7.19	0.787	25.6
49.3	19.4	8.31	16.0	6.56	0.713	22.4
	$\Delta\varepsilon_1$	$\Delta\varepsilon_2$	τ_1 (μs)	τ_2 (ns)		
62.2	7.31	15.7	0.717	19.4		
77.0	6.24	13.1	0.711	16.6		
86.4	11.6	11.2	0.686	17.3		

temperature range, only two subrelaxations were observed which are called subrelaxation 1 and subrelaxation 2.

From the data of relaxation time of each relaxation process in Table IV, it can be concluded that the subrelaxations 2 and 3 at low temperatures correspond to the subrelaxations 1 and 2 at higher temperatures. The continuous changes of the dielectric parameters of subrelaxations 2 and 3 with temperature indicate that the mechanisms of these two subrelaxations do not vary within the studied temperature range. However, the subrelaxation 1 disappears (or becomes vague) with increasing temperature, which may be due to the enlargement of the electrode polarization effect at higher temperature, which masked the subrelaxation 1 at low frequency.

2. Thermodynamic analysis of subrelaxations

Relaxation phenomena could be viewed as a process in which energy changes from one state to another through an energy barrier. From the temperature-dependent dielectric spectra of PAA-g-PEO solutions we can obtain an important kinetic parameter, that is, the relaxation rate constant k which has a reciprocal relationship with the relaxation time ($k = 1/\tau$). Then, the activation enthalpy ΔH and the corresponding entropy ΔS of the three subrelaxation processes can be obtained by the following Eyring equation [41]:

$$\ln(\tau T) = \ln\left(\frac{h}{k_B}\right) - \frac{\Delta S}{R} + \frac{\Delta H}{RT}, \qquad (19)$$

where h denotes the Planck constant, and R and k_B are the gas constant and Boltzmann constant, respectively.

According to Eq. (19), the linear relationships between $\ln(\tau_i T)$ and $1/T$ are expected, where i denotes the serial number of subrelaxation. The plots of $\ln(\tau_i T)$ against $1/T$ for all measurement systems were made and the results for the PAA-g-PEO solutions at a concentration of 0.6 mg/ml
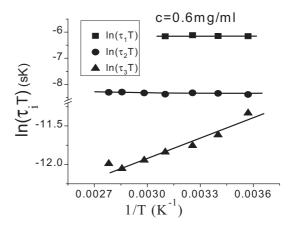

FIG. 9. Plots of $\ln(\tau_i T)$ against $1/T$; solid lines are linear fitting results, taking $c = 0.6$ mg/ml, for example.

are shown in Fig. 9. From the intercept and slope of these lines, ΔH and ΔS were estimated and the results are listed in Table V.

It can be seen in Table V that the activation enthalpy of subrelaxation 3, ΔH_3, was about 7 kJ/mol, which agrees with published values in the range 4–17 kJ/mol [42] where the relaxations are attributed to counterion fluctuation. This result gives support to the mechanism of subrelaxation 3 which originates from the fluctuation of free counterions. The activation enthalpy of the three relaxation processes are all positive (except for the ΔH_2 at $c = 0.6$ mg/ml), indicating the fluctuation of counterions is an endothermic process, because both thermal motion and fluctuation of counterions in the electric field need energy. $\Delta H_3 > \Delta H_1$ (or ΔH_2) implies the fluctuation of free counterions ought to overcome a larger energy barrier compared to the condensed counterions.

Additionally, the activation enthalpies ΔS of the three subrelaxations are all below zero, indicating the environment is cooperative for each relaxation process [43] and the systems are less ordered owing to the directional movements of the counterions. $\Delta S_3 > \Delta S_1$ (or ΔS_2) suggests that the fluctuation of condensed counterions is more prone to diminish the disorder of the solution systems.

V. CONCLUSION AND OUTLOOK

In summary, dielectric properties of aqueous PAA-g-PEO-13% solution have been investigated in the frequency range from 40 Hz to 110 MHz. Three relaxations are observed at about 22 kHz, 220 kHz, and 4 MHz, and their mechanisms are proved by the scaling theory on the fluctuation of counterions. A relaxation process at about 220 kHz is defined

TABLE V. Thermodynamic parameters, ΔH and ΔS, estimated by Eq. (19).

c (mg/ml)	ΔS_1 (J/K/mol)	ΔS_2 (J/K/mol)	ΔS_3 (J/K/mol)	ΔH_1 (kJ/mol)	ΔH_2 (kJ/mol)	ΔH_3 (kJ/mol)
0.01	−138.7	−127.9	−76.32	2.83	0.157	7.70
0.3	−351.8	−121.1	−67.14	0.154	2.17	10.8
0.6	−146.1	−130.2	−78.91	0.0813	−0.597	6.47
2.0	−133.4	−117.1	−76.03	4.20	2.15	5.13

and its mechanism is closely related to the hydrogen-bonding complexes. The findings in this work experimentally support the prediction of the existing scaling theory of counterion fluctuation. Moreover, the activation enthalpy ΔH and the activation entropy ΔS of each subrelaxation were estimated. As to the three relaxation processes, $\Delta H > 0$ implies the fluctuation of counterions is an endothermic process. $\Delta S < 0$ indicates the systems are less ordered and the environment is cooperative for each relaxation process.

The concentration range (from 0.01 to 8.0 mg/ml) in our study was divided into three regions: dilute, unentangled semidilute, and entangled semidilute solution. PEO side chains greatly strengthen the interactions among PAA-*g*-PEO chains, resulting in the chains overlapping at a very low concentration and the formation of a hydrogen-bonding complex.

In conclusion, we think it is very valuable to perform a further study about the effects of multivalent cations on the dielectric spectra of polyelectrolyte solutions, because many theoretical researches have showed that multivalent cations are prone to condense onto the polyelectrolyte chain and significantly change the chain conformation [18,19]. Besides, it should be a challenging issue to explore how the cations of different valance distribute around the polyelectrolyte chain and also to detect the changes in chain conformation from the DRS's point of view.

[1] L. Serra, J. Doménech, and N. A. Peppas, Eur. J. Pharm. Biopharm. **63**, 11 (2006).

[2] H. R. Sondjaja, T. A. Hatton, and K. C. Tam, Langmuir **24**, 8501 (2008).

[3] G. H. Kirby, D. J. Harris, Q. Li, and J. A. Lewis, J. Am. Ceram. Soc. **87**, 181 (2004).

[4] M. Sedlak, M. Antonietti, and H.Cölfen, Macromol. Chem. Phys. **199**, 247 (1998).

[5] V. V. Khutoryanskiy, Int. J. Pharm. **334**, 15 (2007).

[6] H. Cölfen, Macromol. Rapid Commun. **22**, 219 (2001).

[7] K. Nakashima and P. Bahadur, Adv. Colloid Interface Sci. **123–126**, 75 (2006).

[8] S. Holappa, M. Karesoja, J. Shan, and H. Tenhu, Macromolecules **35**, 4733 (2002).

[9] L. N. Gu, Z. Shen, C. Feng, Y. G. Li, G. L. Lu, and X. Y. Huang, J. Polym. Sci., Part A: Polym. Chem. **46**, 4056 (2008).

[10] W. D. Zhang, W. Zhang, Z. P. Cheng, N. C. Zhou, J. Zhu, Z. B Zhang, G. J. Chen, and X. L. Zhu, Macromolecules **44**, 3366 (2011).

[11] J. K. Hao, G. C.Yuan, W. D. He, H. Cheng, C. C. Han, and C. Wu, Macromolecules **43**, 2002 (2010).

[12] S. Holappa, L. Kantonen, F. M. Winnik, and H. Tenhu, Macromolecules **37**, 7008 (2004).

[13] V. V. Khutoryanskiy, A. V. Dubolazov, Z. S. Nurkeeva, and G. A. Mun, Langmuir **20**, 3785 (2004).

[14] A. V. Dobrynin and M. Rubinstein, Prog. Polym. Sci. **30**, 1049 (2005).

[15] R. G. Winkler, M. O. Steinhauser, and P. Reineker, Phys. Rev. E **66**, 021802 (2002).

[16] R. G. Winkler, M. O. Steinhauser, and P. Reineker, New J. Phys. **6**, 11 (2004).

[17] A. G. Cherstvy, J. Phys. Chem. B **114**, 5241 (2010).

[18] J. Kłos and T. Pakula, J. Chem. Phys. **122**, 134908 (2005).

[19] F. Carnal and S. Stoll, J. Phys. Chem. A **116**, 6600 (2012).

[20] R. G. Winkler, M. Gold, and P. Reineker, Phys. Rev. Lett. **80**, 3731 (1998).

[21] H. Schiessel and P. Pincus, Macromolecules **31**, 7953 (1998).

[22] C. Keyes-Baig, M. Mathew, and J. Duhamel, J. Am. Chem. Soc. **134**, 16791 (2012).

[23] F. Bordi, C. Cametti, and R. H. Colby, J. Phys.: Condens. Matter **16**, 1423 (2004).

[24] C. Cametti and S. Zuzzi, J. Phys. Chem. B **114**, 7140 (2010).

[25] K. Ito, A. Yagi, N. Ookubo, and R. Hayakawa, Macromolecules **23**, 857 (1990).

[26] N. Ookubo, Y. Hirai, K. Ito, and R. Hayakawa, Macromolecules **22**, 1359 (1989).

[27] G. S. Manning, J. Chem. Phys. **51**, 924 (1969).

[28] D. J. Bakewell, I. Ermolina, H. Morgan, J. Milner, and Y. Feldman, Biophys. Acta **1493**, 151 (2000).

[29] C. Y. Liu and K. S. Zhao, J. Phys. Chem. B **116**, 763 (2012).

[30] A. V. Dobrynin, R. H. Colby, and M. Rubinstein, Macromolecules **28**, 1859 (1995).

[31] T. Odijk, Macromolecules **12**, 688 (1979).

[32] C. Y. Liu and K. S. Zhao, Soft Matter **6**, 2742 (2010).

[33] H. P. Schwan, in *Physical Techniques in Biological Research*, edited by W. L. Nastuk (Academic Press, New York, 1963), Vol. VIB, pp. 323–407.

[34] P. G. de Gennes, P. Pincus, R. M. Velasco, and F. Brochard, J. Phys. (Paris) **37**, 1461 (1976).

[35] F. Van der Touw, and M. Mandel, Biophys. Chem. **2**, 231 (1974).

[36] A. Minakata, Biopolymers **11**, 1567 (1972).

[37] E. A. Litmanovich, S. O. Zakharchenko, and G. V. Stoichev, J. Phys. Chem. B **111**, 8567 (2007).

[38] C. C. Rojas, K. G. Wahlund, B. Bergenståhl, and L. Nilsson, Biomacromolecules **9**, 1684 (2008).

[39] S. Koneshan, R. M. Lynden-Bell, and J. C. Rasaiah, J. Am. Chem. Soc. **120**, 12041 (1998).

[40] L. Longsworth, J. Phys. Chem. **58**, 770 (1954).

[41] G. Smith, B. Y. Shekunov, J. Shen, A. P. Duffy, J. Anwar, M. G.Wakerly, and R. Chakrabarti, Pharm. Res. **13**, 1181 (1996).

[42] F. Pedone and A. Bonincontro, Biochim. Biophys. Acta **1073**, 580 (1991).

[43] A. V. Sarode and A. C. Kumbharkhane, Polym. Int. **61**, 609 (2012).